Volume 4 | Number 4 | April 2014 | Pages 881–1162

# Catalysis Science & Technology

www.rsc.org/catalysis

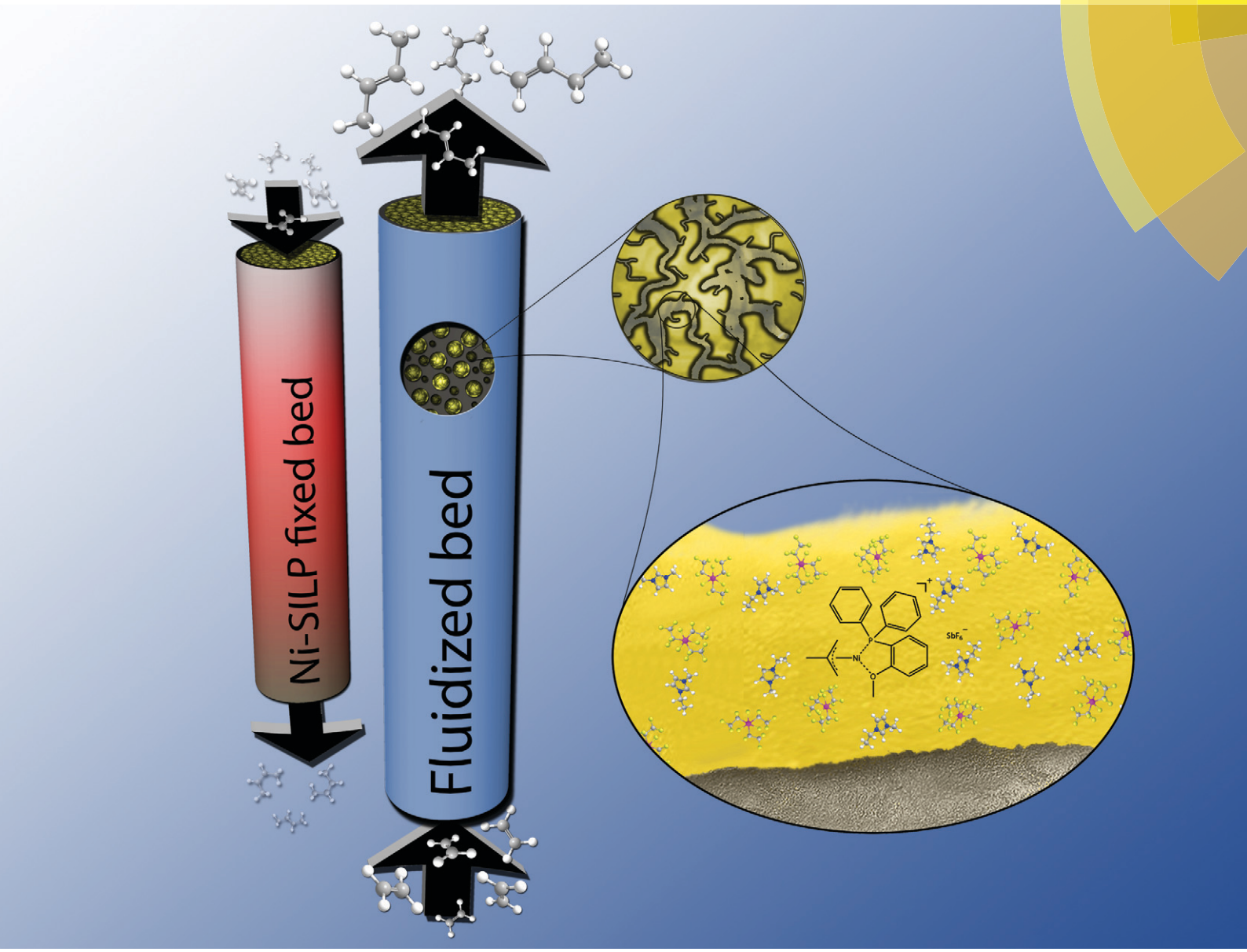


ISSN 2044-4753

ROYAL SOCIETY OF CHEMISTRY

COVER ARTICLE
Haumann, Wasserscheid *et al.*
Dimerization of ethene in a fluidized bed reactor using Ni-based Supported Ionic Liquid Phase (SILP) catalysts

Catalysis Science & Technology

PAPER

View Article Online
View Journal | View Issue



Cite this: *Catal. Sci. Technol.*, 2014, 4, 936

# Dimerization of ethene in a fluidized bed reactor using Ni-based Supported Ionic Liquid Phase (SILP) catalysts†

Florian T. U. Kohler,[a] Konstantin Gärtner,[a] Veit Hager,[a] Marco Haumann,*[a] Michelle Sternberg,[b] Xinjiao Wang,[b] Normen Szesni,[c] Karsten Meyer[b] and Peter Wasserscheid*[a]

Received 8th November 2013,
Accepted 17th December 2013

DOI: 10.1039/c3cy00905j

www.rsc.org/catalysis

The complexes [(mall)Ni(dppanis)][$SbF_6$] (mall = methallyl, dppanis = (2-methoxyphenyl)diphenylphosphine) **1**, [(mall)Ni($PPh_3OC_{10}$)][$SbF_6$] ($PPh_3OC_{10}$ = (2-decyloxyphenyl)diphenylphosphine) **2**, and [(mall)Ni($PPh_3$OdiMePh)][$SbF_6$] ($PPh_3$OdiMePh = (2-(2,6-dimethylphenoxy)phenyl)diphenylphosphine) **3** were immobilized as Supported Ionic Liquid Phase (SILP) catalysts and applied for the tandem dimerization/isomerization of ethylene to 2-butene in a fluidized bed reactor. The better heat removal in the fluidized bed improves the catalyst stability and allows for a more detailed investigation of the deactivation mechanism. Based on kinetic studies, a second order deactivation mechanism is proposed, in which two nickel complexes dimerize if the supply of ethene is insufficient.

## Introduction

Over the last decades, on-purpose routes for the production of propene from ethene (ethene to propene, ETP) have attracted increasing interest due to a shifting demand from polyethylene to polypropylene.[1–3] The ETP sequence involves dimerization of ethene to 1-butene and consecutive isomerization to 2-butene. Metathesis of the formed 2-butene with ethene finally yields propene. Literature known systems for these consecutive reactions include heterogeneous catalysts, such as zeolites, supported molybdenum, tungsten oxide, tungsten hydride or nickel ions loaded on MCM-41.[4–11] We recently reported an immobilized version of cationic, homogeneous nickel complexes that allow the dimerization and isomerization of ethylene to 2-butene with an exceptionally high selectivity.[12] Such nickel complexes were tested in the past for ethylene oligomerization to alpha-olefins but were discarded due to their disadvantageously high isomerization activity.[13] Homogeneous nickel complexes are well known oligomerization catalysts following a nickel hydride chain growth mechanism in which the competition between chain growth and termination *via* β-hydride elimination is governing the product distribution.[14–16] While neutral nickel complexes usually produce higher alkenes in a relative wide Schulz–Flory distribution, short alkenes are mainly obtained with cationic catalysts.[17,18] Amongst those, methallyl nickel complexes, predominantly with phosphinocarboxylates as ligands, display high oligomerization and isomerization activities already at mild temperatures and at low ethylene pressures (see Fig. 1 for the complexes [(mall)Ni(dppanis)][$SbF_6$] (dppanis = (2-methoxyphenyl)diphenylphosphine) **1**, [(mall)Ni($PPh_3OC_{10}$)][$SbF_6$] ($PPh_3OC_{10}$ = (2-decyloxyphenyl)diphenylphosphine) **2**, and [(mall)Ni($PPh_3$OdiMePh)][$SbF_6$] ($PPh_3$OdiMePh = (2-(2,6-dimethylphenoxy)phenyl)diphenylphosphine) **3**).[19–26]

Due to their ionic nature, these nickel complexes can be dissolved in ionic liquids.[27–30] By dispersing the so-obtained ionic catalyst solutions on a highly porous inorganic support, solid materials are obtained that can be handled like classical heterogeneous catalysts.[31,32] These supported ionic liquid phase (SILP) catalysts, depicted in Fig. 2, have been

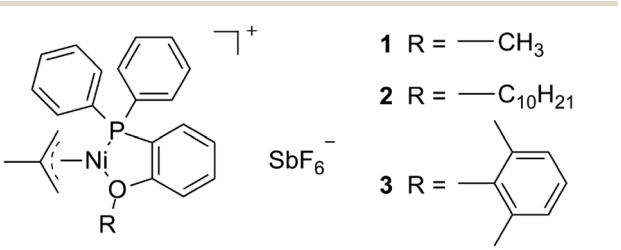


**Fig. 1** Cationic nickel catalyst complexes applied for the tandem dimerization/isomerization of ethene to 2-butene.

[a] *Department of Chemical and Bioengineering, Chemical Reaction Engineering, University Erlangen-Nuremberg, Egerlandstraße 3, D-91058 Erlangen, Germany. E-mail: marco.haumann@fau.de, peter.wasserscheid@crt.cbi.uni-erlangen.de*
[b] *Department of Chemistry and Pharmacy, Inorganic Chemistry, University Erlangen-Nuremberg, Egerlandstraße 1, D-91058 Erlangen, Germany*
[c] *Clariant Produkte (Deutschland) GmbH, Waldheimer Straße 13, D-83052 Bruckmühl, Germany*

† Electronic supplementary information (ESI) available. See DOI: 10.1039/c3cy00905j

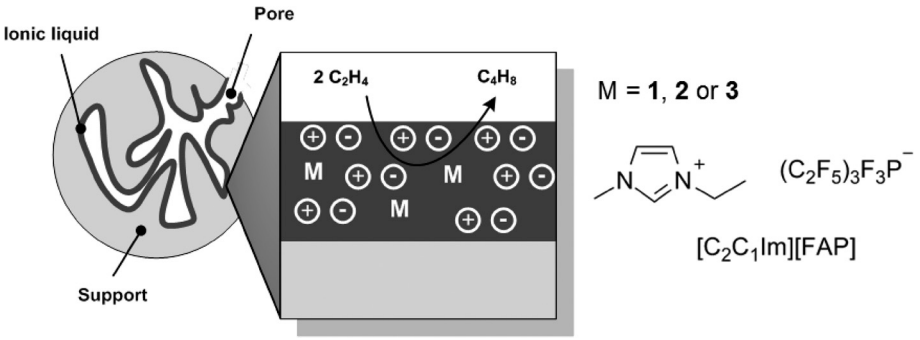


Fig. 2 Schematic representation of the applied Ni-based SILP catalyst systems.

applied in a variety of reactions, both in liquid and gas phase contact.[33] Due to the extremely low volatility of ionic liquids, the SILP concept is ideally suited for continuous gas-phase processes.[34]

For the gas-phase dimerization/isomerization of ethene in the presence of the cationic Ni-SILP catalysts **1** to **3**, the complexes were dissolved in the ionic liquid $[C_2C_1Im][FAP]$ (see Fig. 2) and dispersed as a thin film over a silica gel 100 support.[12] These SILP catalysts showed high activity in the first phase of the reaction, exemplified by an initial turn-over frequency $TOF_0$ of around 520 $mol_{butene}\ mol_{Ni}^{-1}\ h^{-1}$. Catalyst stabilities were reasonable and reached overall turn-over numbers (TONs) ranging from 53 300 (for complex **1**) to 97 700 (for complex **3**) at 19 °C. The low reaction temperature was required to avoid thermal decomposition of the cationic Ni-complexes.[35] Under these conditions, the combination of high catalytic activity and strong exothermicity of the dimerization reaction still resulted in hot spot formation inside the fixed catalyst bed. The temperature at the top end of the fixed bed ($T_{top}$) and at the bottom end of the fixed bed ($T_{bottom}$) were measured over time using two thermocouples (Fig. 3). At the beginning of the reaction, a severe rise in temperature to $T_{top}$ = 59 °C was observed, while the temperature at the bottom end increased to only 42 °C. After that, the temperature at the top rapidly decreased approximating the cooling temperature $T_c$ while the temperature at the bottom end slowly increased. With concomitant approach of the maximum temperature at the bottom of $T_{bottom}$ = 56 °C, a drop in conversion occurred. The observed course of temperature indicates deactivation of the catalyst by a migrating reaction–deactivation front as schematically depicted in Fig. 3. This front obviously first develops at the top end of the fixed bed reactor where ethene comes in contact with the catalyst bed. Due to the high activity of the applied cationic nickel complexes, full conversion of ethene occurs in this upmost layer of the fixed bed. Accordingly, the major part of the reaction heat ($\Delta H_R$ = −112.3 kJ $mol^{-1}$) is released in this layer and a temperature hot spot forms resulting in the thermal deactivation of the dissolved Ni-complex.

Once a certain layer of the catalyst bed has been deactivated the reaction front moves to the next layer, again, inducing a rise in temperature followed by thermal catalyst deactivation. In this manner, a reaction–deactivation front migrates through the entire fixed bed until it reaches the bottom and the whole system turns inactive.

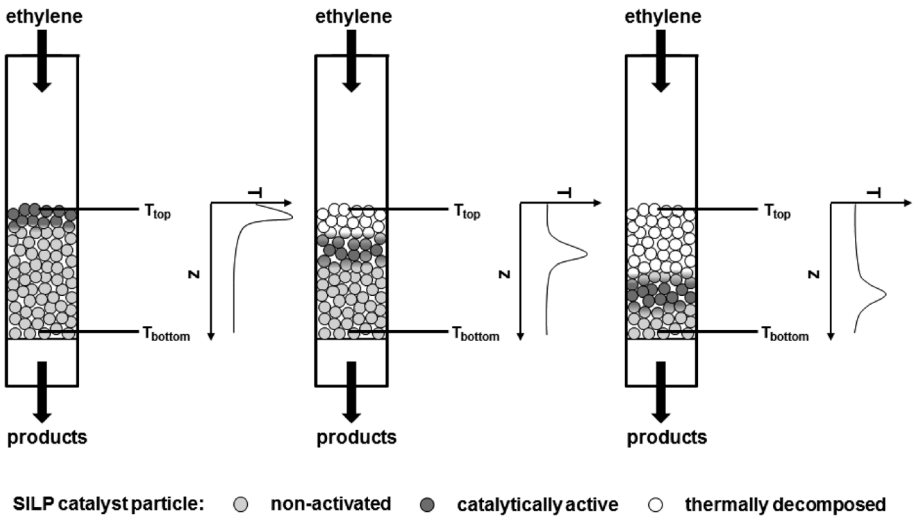


Fig. 3 Schematic representation of the reaction/deactivation front moving through the fixed bed containing the SILP catalyst.

Remarkably, these hot spot formation problems could not be improved by diluting the SILP catalyst with an inert material, lowering the nickel content, or increasing the content of the inert gas in the reaction mixture. Note that the failure of all these well-established ways to circumvent hot spots in fixed bed reactors is linked to the extreme sensitivity of cationic Ni-complexes against humidity and all traces of nucleophiles that may act as strong catalyst poisons.

In the present work we report on the application of fluidized bed reactor technology to improve the heat removal from the SILP catalyst. It is anticipated that increased isothermicity in the reactor will lead to prolonged catalyst stability. To the best of our knowledge, the here described work represents the first attempt to apply SILP catalysts in a fluidized bed reactor.

## Results and discussion

### Fluidization behavior of silica based support materials

We first conducted a detailed characterization of appropriate $SiO_2$-based porous support materials and their fluidization behavior in a nitrogen carrier flow. An overview of the tested support materials and their characteristics is given in Table 1. The measured particle size distribution, bulk density, and minimum fluidization velocities of the support materials applied in a fluidized bed reactor are listed as well.

In 1973, Geldart classified four different groups of solids applied in gas–solid fluidized beds based on their fluidization behavior.[38] Group A solids are aeratable and form a homogenous fluidized bed, whereas group B particles lead to rising gas bubbles inside the fluidized bed. Group C particles are very small and cohesive and thus fluidization is hardly realizable. Particles related to group D are relatively huge and fluidized beds tend to build a spouted bed with gas channels. From the Geldart classification of our support materials shown in Fig. 4 (left), it became obvious that some supports (**S2**, **S5**, **S6** and **S12**) can be classified as part of Geldart group A, while most $SiO_2$-based porous supports are in the boundary region between Geldart groups A and B (**S1**, **S3**, **S4**, **S8**, **S10** and **S11**). Only **S7** can clearly be assigned to Geldart B, most likely forming a bubbling fluidized bed. These results were confirmed by the pressure drop curves of the investigated materials given in the ESI.† The minimum fluidization velocity $v_{mf,meas}$ determined for these materials indicated also the best fluidization performance for supports **S5** and **S11** (entries 5 and 11). The measured values are in the range of the predicted minimum fluidization velocity $v_{mf,calc}$ calculated according to the literature procedure[36,37] (for the equation see the ESI†).

In consecutive fluidization experiments we were interested in the change of the fluidization characteristics of SILP-systems compared to those of the respective neat support materials. We therefore prepared SILP-particles based on **S5** with different amounts of the ionic liquid 1-ethyl-3-methylimidazolium tetrafluoroborate ($[C_2C_1Im][BF_4]$). The measured pressure drop curves of **S5** and the SILP-systems based on **S5** with pore filling degrees of $\alpha_{IL}$ = 0.3, 0.6 and 0.9 are shown in Fig. 4 (right). The results indicate that with a higher ionic liquid loading both the overall pressure drop and the minimum fluidization velocity ($v_{mf}$ from 0.16 cm $s^{-1}$ for $\alpha_{IL}$ = 0 to 0.20 cm $s^{-1}$ for $\alpha_{IL}$ = 0.9) are increasing. A homogenous fluidization, however, is still possible using **S5** with an ionic liquid pore filling of $\alpha_{IL}$ = 0.9 of $[C_2C_1Im][BF_4]$. Obviously the Geldart classification specifies these SILP-systems to behave still like Geldart A particles.

In a preliminary catalytic experiment we investigated the performance of the SILP catalyst (**S5**, $[C_2C_1Im][FAP]$, $\alpha_{IL}$ = 0.3, Ni-loading = 0.25 wt.%) in a fluidized bed reactor using an undiluted ethene flow as feedstock at a flow rate of 25.5 Nml $min^{-1}$. An incomplete fluidization of the fluidized SILP bed was observed, caused by the decrease of the volume flow due to volume contraction during the dimerization reaction. Additionally, the condensation of high-boiling by-products, mainly hexenes and octenes, in the porous SILP material turned out to be a severe drawback; consequently, the SILP particles agglomerated in the course of the experiment. Increasing the volume flow of ethene to 51 Nml $min^{-1}$ gave also an undesirable result, as the temperature inside the

**Table 1** Characteristics of $SiO_2$-based porous support materials and their minimum fluidization velocity $v_{mf}$ for the fluidization in a nitrogen flow

| Entry | Support | $V_{pore}$ [a] / ml $g^{-1}$ | $S_{BET}$ [b] / $m^2$ $g^{-1}$ | $d_{pore}$ [c] / nm | $\delta$ [d] / g $cm^{-3}$ | $x_{50}$ [e] / μm | $v_{mf,meas}$ [f] / cm $s^{-1}$ | $v_{mf,calc}$ [g] / cm $s^{-1}$ |
|---|---|---|---|---|---|---|---|---|
| 1 | **S1**[h] | 0.455 | 111.9 | 13.9 | 3.203 | 68.5 | 0.25 | 0.18 |
| 2 | **S2**[h] | 0.578 | 216.6 | 17.3 | 2.525 | 58.7 | 0.11 | 0.09 |
| 3 | **S3**[h] | 0.958 | 182.3 | 12.6 | 2.356 | 98.8 | 0.21 | 0.28 |
| 4 | **S4**[h] | 0.732 | 191.4 | 9.1 | 2.664 | 89.0 | 0.35 | 0.26 |
| 5 | **S5**[h] | 0.732 | 296.2 | 7.0 | 2.129 | 56.0 | 0.16 | 0.08 |
| 6 | **S6**[h] | 0.784 | 229.5 | 8.8 | 2.104 | 57.0 | 0.17 | 0.08 |
| 7 | **S7**[h] | 0.972 | 346.2 | 11.0 | 2.650 | 123.8 | 0.37 | 0.57 |
| 8 | **S8**[i] | 0.483 | 180.3 | 4.7 | 1.921 | 120.9 | n.d. | 0.34 |
| 9 | **S9**[j] | 1.392[k] | 45.7[k] | 130[k] | 2.218 | 80.7 | 0.11 | 0.18 |
| 10 | **S10**[j] | 1.381[k] | 54.4[k] | 57.7[k] | 2.489 | 95.1 | 0.22 | 0.24 |
| 11 | **S11**[j] | 1.392[k] | 45.7[k] | 130[k] | 2.218 | 47.8 | 0.10 | 0.06 |
| 12 | **S12**[i] | 0.855 | 346.5 | 7.0 | 2.070 | 59.5 | 0.17 | 0.09 |

[a] Pore volume. [b] Surface area according to BET method. [c] Average pore diameter. [d] Density. [e] Mean particle size. [f] Minimum fluidization velocity, measured. [g] Minimum fluidization velocity, calculated according to ref. 36 as summarized in ref. 37. [h] Supplied by Clariant. [i] Purchased from Merck KgaA. [j] Purchased from VitraBio. [k] Manufacturer's data by means of mercury intrusion method.

 

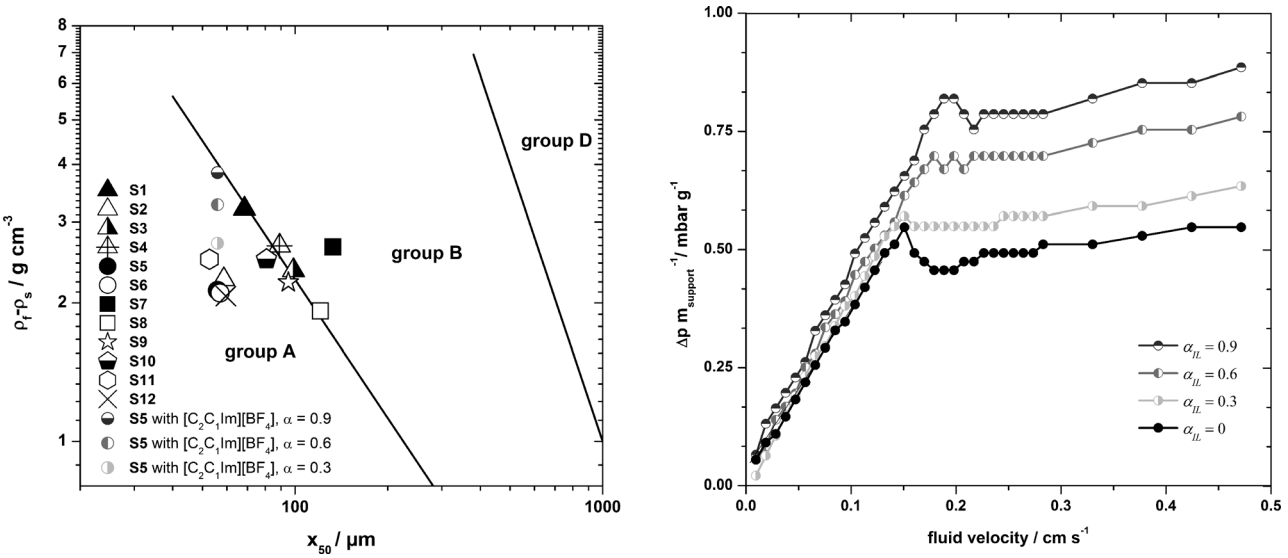


**Fig. 4** Left: Classification of porous support materials according to Geldart;[38] mean particle size from particle size distribution and solid density. Right: Specific pressure drop curves of the support **S5** ($\alpha_{IL}$ = 0) and SILP-systems consisting of **S5** with different pore fillings of $[C_2C_1Im][BF_4]$ ($\alpha_{IL}$ = 0.3, 0.6 and 0.9); $m_{bed}$ = 5 g, $d_i$ = 16 mm, and $V_{nitrogen}$ = 2–100 ml min$^{-1}$.

catalyst bed instantaneously rose to around 353 K. This could be attributed to the high exothermicity of the dimerization reaction, leading to an immediate deactivation of the temperature sensitive Ni catalyst. In successive experiments we therefore diluted the ethylene feed with argon in order to sustain the fluidization of the SILP catalyst bed. Under these conditions, no temperature increase was detectable while the fluidization of the catalyst bed was conserved. Details of these preliminary experiments are given in the ESI.†

### Comparison of fixed bed and fluidized bed dimerization

The dimerization of two diluted ethene substrate flows, purified and non-purified (for details see the ESI†), in both fixed bed and fluidized bed operations of the reactor was investigated and Table 2 compiles the parameters of the SILP catalysts, the reaction conditions, and the catalytic results (entries 14–17). Fig. 5 (left) shows the comparison of both operation modes by showing the conversion and selectivity over time-on-stream (TOS).

**Table 2** SILP catalyst composition, reaction conditions and results from fluidized bed dimerization experiments

| Entry | Support | $w_{Ni}$[a] wt.‰ | $m_{SILP}$[b] g | $T_{reactor}$ K | $p_{ethene}$ $10^{-3}$ bar | $TOF_{max}$ $mol_{butene}$ $mol_{Ni}^{-1}$ $h^{-1}$ | $t_{1/2}$[c] h | $TON_{1/2}$ $mol_{butene}$ $mol_{Ni}^{-1}$ |
|---|---|---|---|---|---|---|---|---|
| 13 | **S5** | 2.50[d] | 1 | 292 | 68 | 181 | 10.9 | 1550 |
| 14 | **S5** | 2.50[e] | 1 | 292 | 68 | 189 | 34.2 | 4280 |
| 15 | **S5** | 2.50[f] | 1 | 292 | 68 | 215 | 49.0 | 8040 |
| 16 | **S5** | 2.50 | 1 | 292 | 68 | 174 | 132 | 15 500 |
| 17 | **S5** | 2.50 | 0.2 | 292 | 68 | 913 | 21.4 | 11 300 |
| 18 | **S6** | 2.50 | 0.2 | 292 | 68 | 860 | 21.4 | 12 300 |
| 19 | **S7** | 2.50 | 0.2 | 292 | 68 | 870 | 9.3 | 5420 |
| 20 | **S11** | 2.60 | 0.2 | 292 | 68 | 954 | 28.9 | 18 000 |
| 21 | **S5** | 2.50 | 0.2 | 292 | 17 | 185 | 29.8 | 3740 |
| 22 | **S5** | 2.50 | 0.2 | 292 | 34 | 364 | 29.3 | 7430 |
| 23 | **S5** | 2.50 | 0.2 | 292 | 136 | 1644 | 15.7 | 18 300 |
| 24 | **S5** | 1.25[g] | 0.2 | 292 | 68 | 441 | 7.8 | 2890 |
| 25 | **S5** | 1.88[g] | 0.2 | 292 | 68 | 388 | 16.6 | 4630 |
| 26 | **S5** | 2.50[g] | 0.2 | 292 | 68 | 420 | 19.8 | 5370 |
| 27 | **S5** | 3.13[g] | 0.2 | 292 | 68 | 409 | 16.1 | 4590 |
| 28 | **S5** | 2.50 | 0.2 | 282 | 68 | 1010 | 27.9 | 1850 |
| 29 | **S5** | 2.50 | 0.2 | 302 | 68 | 774 | 15.8 | 8000 |
| 30 | **S5** | 2.50 | 0.25[h] | 292 | 68 | 714 | 24.5 | 11 600 |
| 31 | **S5** | 2.50 | 0.31[i] | 292 | 68 | 640 | 62.0 | 27 100 |

Standard conditions: $[C_2C_1Im][FAP]$, $\alpha_{IL}$ = 0.3; $V_{ethene}$ = 5.1 Nml min$^{-1}$, $\tau \approx$ 1.3 s.[a] Nickel loading related to the support. [b] Total mass of the catalyst in the reactor. [c] Time to reach 50% initial conversion. [d] Fixed bed, feed not purified. [e] Fluidized bed, feed not purified. [f] Fixed bed, feed purified. [g] Other charge of nickel precursor. [h] $\alpha_{IL}$ = 0.6. [i] $\alpha_{IL}$ = 0.9.

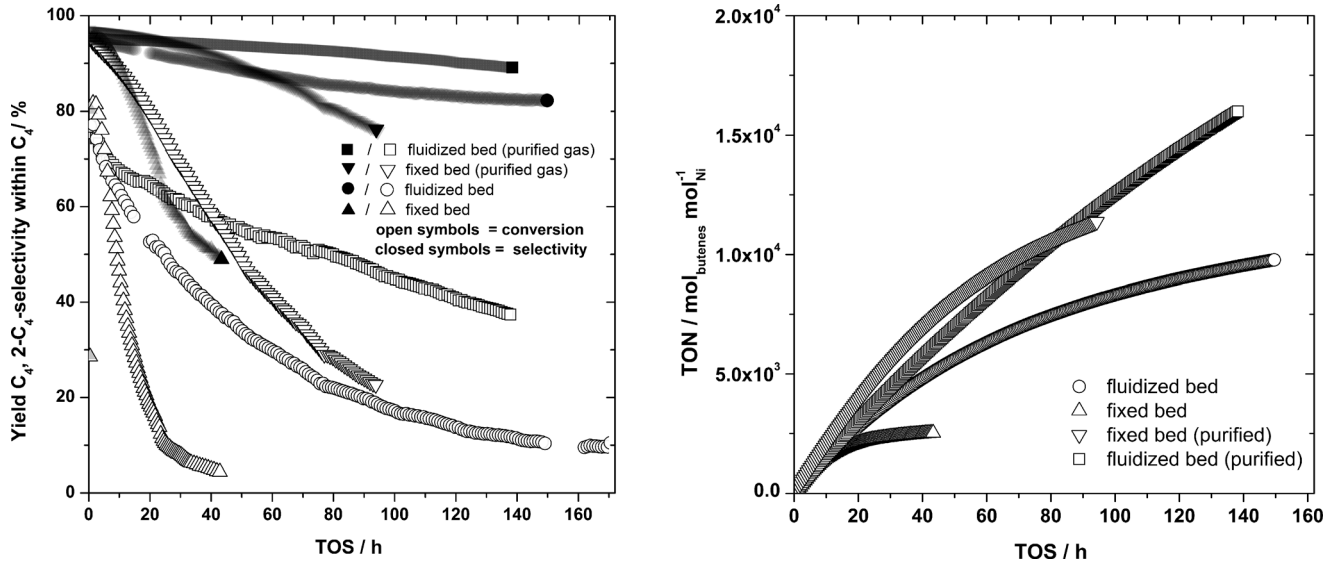


Fig. 5 Comparison of conversion, selectivity of 2-butenes within the $C_4$-fraction and TON of fixed and fluidized bed dimerization of purified and non-purified diluted ethene streams with the SILP catalyst [(mall)Ni-dppanis][$SbF_6$] **1**, $w_{Ni}$ = 2.50 $mg_{Ni}$ $g_{support}^{-1}$, **S5**, [$C_2C_1$Im][FAP], $\alpha_{IL}$ = 0.3; $m_{SILP}$ = 1000 mg, $T_{reactor}$ = 292 K, $p_{ethene}$ = 68 mbar, $V_{ethene}$ = 5.1 Nml $min^{-1}$, $\tau \approx$ 1.3 s, and $p_{reaction}$ = 1 bar.

The results for both feeds (purified and non-purified ethene and argon) show a significant difference between the fixed bed and fluidized bed operation, as expected. The fixed bed experiment with non-purified feeds (entry 13, Table 2) showed a constant conversion level of above 80% for 3 h, followed by a pronounced decrease of conversion within the next 20 h. This deactivation was accompanied by a distinct decrease of the 2-butene selectivity, which dropped from 95% to 75% at the residual conversion of 20%. The turn-over number at 50% activity $TON_{t1/2}$ was $1.55 \times 10^3$ $mol_{butene}$ $mol_{Ni}^{-1}$. In contrast, the fluidized bed experiment (entry 14) showed not only an instantaneous decrease of the conversion of ethene, but also a prolonged deactivation time to reach a residual conversion of 20% at which the 2-butene selectivity was still 85%. The $TON_{t1/2}$ was almost 2.8 times higher than for the comparable fixed bed experiment. This indicates an improved distribution of the released reaction heat throughout the fluidized catalytic bed. Within the fixed bed experiment hot spots are formed, resulting in a faster deactivation due to the temperature sensitivity of the Ni catalyst.

The two reactor types also gave different results when using purified (ethene and argon with $H_2O$ and $O_2 \leq 15$ ppb) instead of standard feed with the latter yielding lower stability. In the fixed bed (entry 15, Table 2) the catalyst showed a higher initial activity compared to standard feed and the long-term stability of the fluidized bed experiment (entry 16, Table 2) was higher. The turn-over number (TON) over time-on-stream TOS, shown in Fig. 5 (right), demonstrates the improved stability of the SILP catalysts used in a fluidized bed reactor, as these TON values exceed the TON of the corresponding fixed bed experiment by almost a factor of two. Moreover, the better stability with purified gas suggests at least one additional deactivation mechanism besides the thermal decomposition. This deactivation mechanism obviously involves impurities in the feed streams, such as traces of oxygen or moisture.

Although the use of purified ethene feed gas in combination with a fluidized bed instead of a fixed bed improved the activity and stability of the Ni-SILP catalyst, the deactivation process could not be suppressed completely. We therefore investigated the effect of different support materials on the deactivation behavior of the SILP catalyst in a fluidized bed operation.

### Support material variation

In this set of experiments we focused on the supports exhibiting a good fluidization behavior, namely **S5**, **S6** and **S11** and the Geldart B support **S7** as a reference support material (entries 17–20, Table 2). Fig. 6 compiles the obtained TOF and TON over TOS data for the different SILP catalysts with a constant Ni content of $w_{Ni}$ = 2.50 $mg_{Ni}$ $g_{support}^{-1}$.

The **S7** based SILP catalyst (entry 19) formed a bubbling fluidized bed at the given flow parameters; consequently, the SILP catalyst based on the latter showed the poorest stability and thus the lowest $TON_{t1/2}$ of 5420 $mol_{butene}$ $mol_{Ni}^{-1}$ and the lowest TON after 40 h of 13 800 due to locally high ethene concentration and thus – presumably – to higher temperatures. Both SILP catalysts with the almost identical supports **S5** and **S6** showed approximately the same catalytic performance (entry 17 and 18) with slight advantages in activity and stability for the latter. The **S11** based SILP catalysts (entry 20) showed the slowest deactivation with a half-life time of nearly 29 h and also the highest TOF of 954 $mol_{butene}$ $mol_{Ni}^{-1}$ $h^{-1}$. As a consequence, this catalyst gave the highest $TON_{t1/2}$ of 18 000 $mol_{butene}$ $mol_{Ni}^{-1}$ and a final TON after 40 h of almost 25 000 $mol_{butene}$ $mol_{Ni}^{-1}$. Although the TOF of the **S11** based SILP exceeded the TOF found for **S5**, **S6** and **S7**, the effective

 

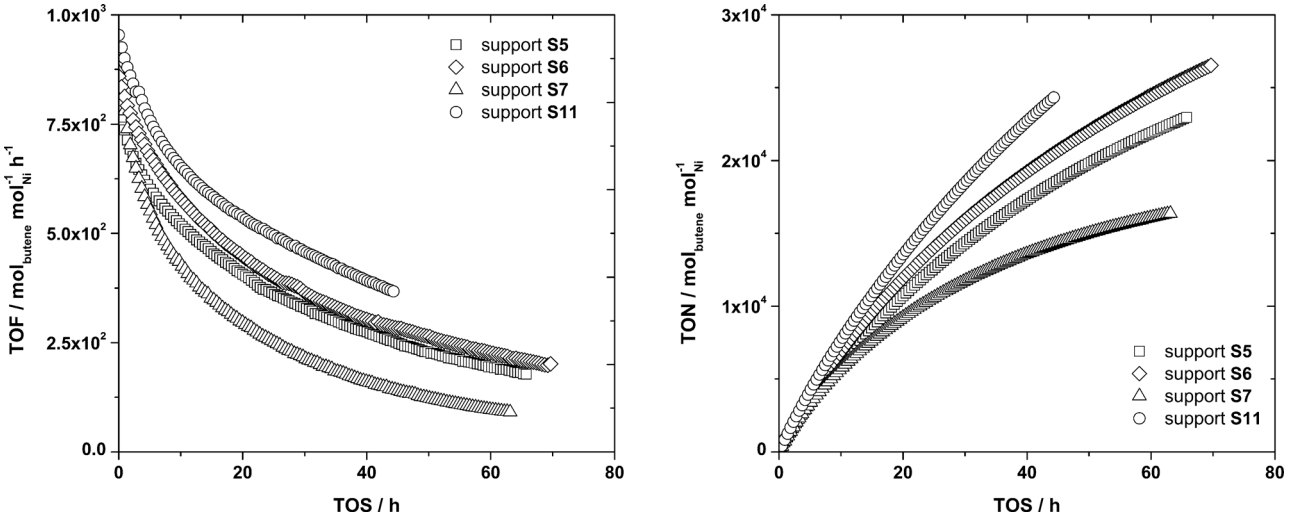


**Fig. 6** TOF and TON over TOS of the ethene dimerization with the SILP catalyst ([(mall)Ni-dppanis][$SbF_6$] **1**, $w_{Ni}$ = 2.50 $mg_{Ni}$ $g_{support}^{-1}$, [$C_2C_1$Im][FAP], $\alpha_{IL}$ = 0.3) with different support materials **S5**, **S6**, **S7** and **S11** in a fluidized bed reactor; $m_{SILP}$ = 200 mg, $T_{reactor}$ = 292 K, $p_{ethene}$ = 68 mbar, $V_{ethene}$ = 5.1 Nml $min^{-1}$, $\tau \approx 0.3$ s, and $p_{reaction}$ = 1 bar.

reaction rate related to the catalytic volume of the **S11** based catalyst was around 1.5 to 2 times lower than the reaction rates for the other supports. This specific difference probably resulted from the differing inner surface, pore volume, and pore diameter of the supports **S11**, **S5**/**S6**, and **S7** (see Table 1). As a result of the smaller inner surface and the different pore volumes, the thickness of the IL film inside the pores was increased. With a constant pore filling degree the theoretical film thickness was one order of magnitude higher using **S11** (7.64 nm) compared to **S5** (0.72 nm). Additionally, the calculated concentration of the Ni-precursor dissolved in the dispersed IL was varied in order to keep $w_{Ni}$ constant. For **S11** based SILP catalysts 102 mol $m_{IL}^{-3}$ were used, while for **S5** systems 198 mol $m_{IL}^{-3}$ were required. Regarding the achievable TON values for the different catalysts it seemed to be advantageous to have Geldart A porous supports with a high pore volume and lower inner surface, since the effective reaction rate related to the catalytic volume was decreased. Obviously, the smaller reaction heat released can then be more effectively distributed throughout the catalyst bed. Regarding this aspect increasing the pore filling should result in a similar effect on the deactivation process.

### Variation of pore filling degree

Entries 17, 30, and 31 in Table 2 summarize the ethene dimerization performance of Ni-SILP catalysts with different pore fillings of $\alpha_{IL}$ = 0.3, 0.6 and 0.9. In these investigations the TOF of the catalysts as well as the volume specific reaction rate were reduced as a consequence of the increase in pore filling of the SILP catalysts. The catalyst with a pore filling of $\alpha_{IL}$ = 0.3 (entry 17) showed the highest activity with a $TOF_{max}$ of 913 $mol_{butene}$ $mol_{Ni}^{-1}$ $h^{-1}$ that was lowered for $\alpha_{IL}$ = 0.6 (entry 30) to a $TOF_{max}$ of 714 $mol_{butene}$ $mol_{Ni}^{-1}$ $h^{-1}$ and for $\alpha_{IL}$ = 0.9 (entry 31) to a $TOF_{max}$ of 640 $mol_{butene}$ $mol_{Ni}^{-1}$ $h^{-1}$. Since the Ni loading was kept constant at $w_{Ni}$ = 2.50 $mg_{Ni}$ $g_{support}^{-1}$, this trend reflects the lower nickel concentration in the ionic liquid film and the influence of mass transport limitations, in particular limitations due to the increasing thickness of the relatively viscous ionic liquid film. In fact, the effective reaction rate is reduced by the decrease of the mass transfer area inside the SILP catalyst pellet and by the longer diffusional path lengths of the substrate in the thicker ionic liquid film. The BET surface area of the particular SILP catalysts is linearly lowered due to an increase of the pore filling.

Interestingly, this lower activity of the nickel catalyst in the ionic liquid film resulted in an improved stability of the SILP material, since a lower reaction rate is naturally accompanied with less heat generation. Also, the thicker film could distribute the reaction heat much better in the liquid phase, thereby stabilizing the temperature sensitive nickel complex. Using the SILP material with the thickest ionic liquid film, a total TON of 27 100 was obtained, which clearly demonstrates the improved stability.

### Variation of nickel loading

To test the influence of mass transport limitation, we varied the specific amount of the complex Ni-dppanis related to the neat support material from 0.125 wt.% to 0.313 wt.% (entry 24–27). Thereby the concentration of Ni inside the IL film was altered from 99.35 mol $m_{IL}^{-3}$ to 248.37 mol $m_{IL}^{-3}$. Fig. 7 displays the volume specific effective reaction rate over TOS as well as the dependency of the initial effective reaction rate on the catalyst complex concentration of the four named experiments.

While the maximum TOF values of these experiments stayed in the same range of 388 to 441 $mol_{butene}$ $mol_{Ni}^{-1}$, the effective reaction rate increased with increasing amount of the Ni precursor. The reaction order with respect to Ni

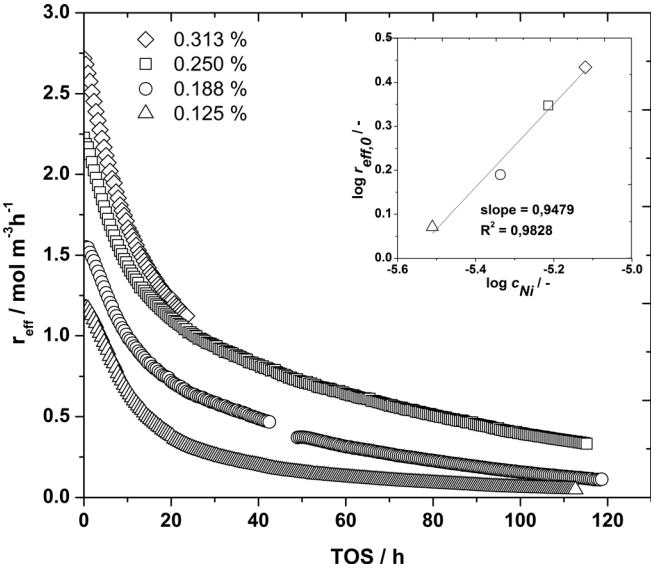


Fig. 7 Effective reaction rate over TOS of SILP catalysts comprising [(mall)Ni-dppanis][$SbF_6$] **1**, [$C_2C_1$Im][FAP], **S5**, $\alpha_{IL}$ = 0.3 with different Ni-loadings $w_{Ni}$ = 1.25, 1.88, 2.50 and 3.13 $mg_{Ni}$ $g_{support}^{-1}$ in a fluidized bed reactor; $m_{cat}$ = 200 mg, $V_{ethene}$ = 5.1 Nml $min^{-1}$, $\tau \approx 0.3$ s, $T$ = 292 K, and $p_{reaction}$ = 1 bar.

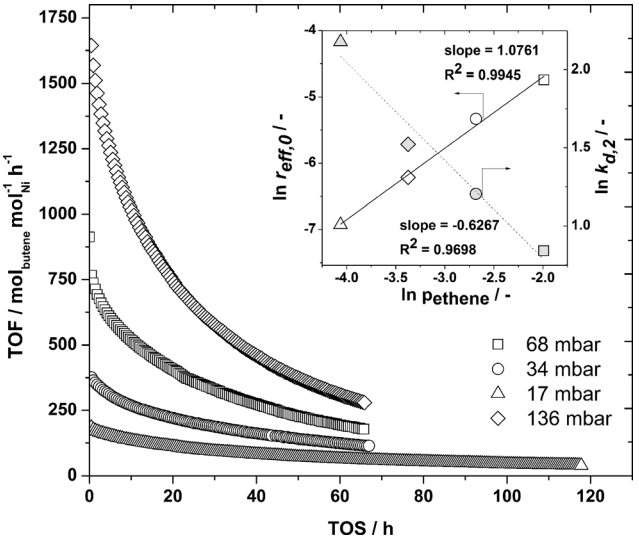


Fig. 8 Turn over frequency over time-on-stream of the standard SILP catalyst at different partial pressures of ethene in a fluidized bed reactor. Inset: determination of the reaction order of ethene by linearization of the initial effective reaction rate and dependency of the deactivation coefficient $k_{d,2}$ on the ethene pressure; [(mall)Ni-dppanis][$SbF_6$] **1**, $w_{Ni}$ = 2.50 $mg_{Ni}$ $g_{support}^{-1}$, [$C_2C_1$Im][FAP], **S5**, $\alpha_{IL}$ = 0.3; $m_{cat}$ = 200 mg, $V_{ethene}$ = 1.28–10.2 Nml $min^{-1}$, $\tau \approx 0.3$ s, $T$ = 292 K, and $p_{reaction}$ = 1 bar.

could be determined as a nearly first order reaction, indicating the absence of mass transport influence at this low ionic liquid loading. The longest half life time, and thus also the highest $TON_{t1/2}$ was identified for the catalyst with a Ni loading of $w_{Ni}$ = 0.250 wt.%. Based on the assumption that lower reaction rates of diluted systems result in higher stability, this effect was probably counterbalanced by oxygen and water impurities still present in the purified feed gas, leading to faster deactivation of the catalyst with lower concentration of nickel.

### Variation of ethene partial pressure

Applying the standard SILP catalyst at 292 K, the partial pressure of ethene was varied by adjusting the volume flow of ethene while keeping the total volume flow and residence time constant. Fig. 8 depicts the measured TOF over TOS for four different partial pressures of ethene ranging from 17 mbar to 136 mbar and the resulting reaction order of ethene calculated from the initial effective reaction rate and the corresponding deactivation parameter $k_{d,2}$ (entries 17 and 21–23).

The differential analysis of $\ln(r_{eff})$ *vs.* $\ln(p_{ethene})$ (see inset) indicates a first order reaction of ethene. We additionally noticed an influence of the partial pressure on the deactivation, exemplified by the deactivation parameter $k_{d,2}$ (for details see the next section). Surprisingly, the deactivation seemed to be decelerated with increasing partial pressure of ethene, since $k_{d,2}$ decreased while $TON_{t1/2}$ increased. This observation is in conflict with the assumption that a slower reaction rate would result in a reduction of the released reaction heat and would therefore result in an improved stability of the Ni-SILP catalyst. We interpret this result as a hint for an additional deactivation mechanism of the cationic Ni-dppanis complex apart from thermal decomposition and poisoning by gas impurities. Our observation would be in line with the assumption of a deactivation route involving the reaction of two active Ni complexes with one another in case insufficient ethene is present.[35] This aspect will be developed in more detail below.

### Deactivation kinetics and modeling

The deactivation behavior of cationic Ni SILP-type catalysts based on the support **S5** was studied in more detail under a fluidized bed operation in a diluted ethene stream in the range of 282 to 302 K. The applied temperature range was restricted by the temperature sensitivity of the catalyst and by the agglomeration of SILP catalyst particles as a consequence of oligomer condensation in the catalytic fluidized bed at very low temperatures. For a first order reaction of ethene and the Ni-complex, the time dependent effective reaction rate can be described using eqn (1).

$$r_{eff}(t) = k'_{eff} \cdot c_{Ni}(t) \text{ with } k'_{eff} = k_{eff} \cdot c_{ethene} \quad (1)$$

For a first order deactivation mechanism, the amount of Ni is reduced within the reaction time $t$ according to eqn (2). The effective reaction rate drops according to eqn (3).

$$c_{Ni}(t) = c_{Ni,0} \cdot e^{-k_{d,1}t} \quad (2)$$

$$r_{eff}(t) = r_0 \cdot e^{-k_{d,1}t} \quad (3)$$

Alternatively, a second order deactivation mechanism can be considered, leading to the effective reaction rate represented by eqn (4) and (5), respectively.

 

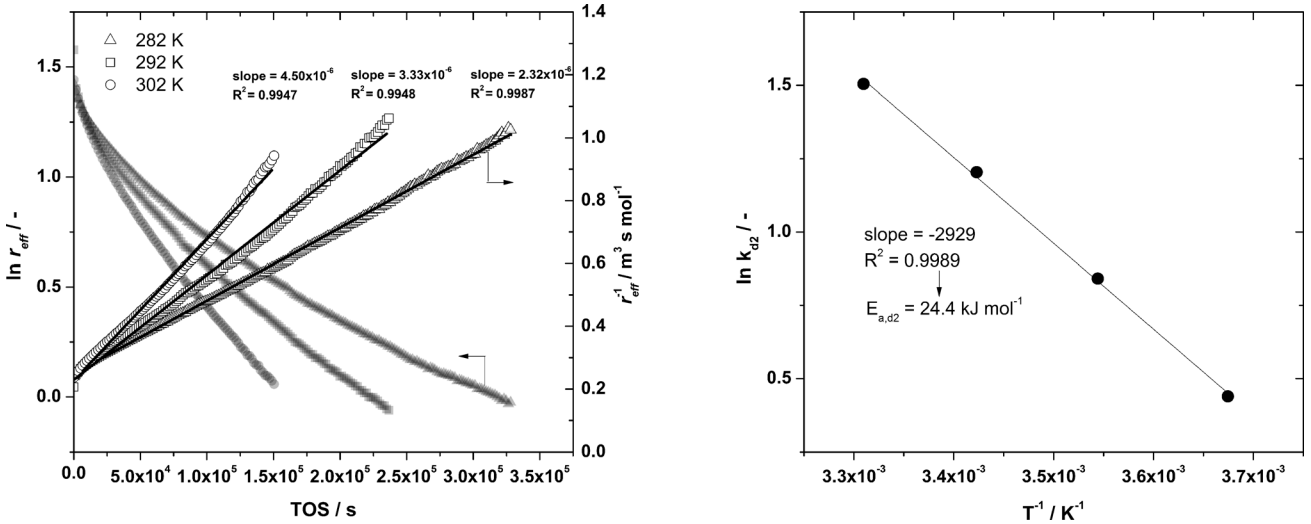


**Fig. 9** Determination of the deactivation coefficients $k_{d,1}$ for the assumption of a first order catalyst deactivation process and $k_{d,2}$ for the assumption of a second order catalyst deactivation process at three different temperatures, 282, 292 and 302 K, and determination of the activation energy of deactivation; SILP catalysts with [(mall)Ni-dppanis][$SbF_6$] **1** complex, $w_{Ni}$ = 2.50 $g_{Ni}$ $g_{support}^{-1}$, **S5**, [$C_2C_1$Im][FAP], $\alpha_{IL}$ = 0.3; $m_{SILP}$ = 200 mg, $p_{ethene}$ = 68 mbar, $V_{ethene}$ = 5.1 Nml $min^{-1}$, $t \approx 0.3$ s, and $p_{reaction}$ = 1 bar.

$$\frac{1}{c_{Ni}(t)} = \frac{1}{c_{Ni,0}} + k_{d,2}t \quad (4)$$

$$\frac{1}{r_{eff}(t)} = \frac{1}{r_{eff,0}} + k_{a,2}t \quad (5)$$

Fig. 9 displays the experimental dimerization result in the form of eqn (3) and (5). The graphs have been obtained by plotting ln $r_{eff}$ and $r_{eff}^{-1}$ *versus* TOS. The slope of the three experiments with different temperatures represents the deactivation constant $k_{d,1}$ (ln $r_{eff}$ over TOS) for a first order deactivation and $k_{d,2}$ ($r_{eff}^{-1}$ over TOS) for a second order deactivation.

While the plot of the logarithmic $r_{eff}$ deviates strongly from linearity, $r_{eff}^{-1}$ matches with a coefficient of determination of $R^2 > 0.994$; the linear behavior required by the deactivation model indicates a second order deactivation process. With the deactivation constant $k_{d,2}$ at four different temperatures (one additional experiment at 272 K is shown in the ESI†), an activation energy of deactivation $E_{A,d}$ of 23.2 kJ $mol^{-1}$ can be determined. A consequence of this relatively low value is that it is not possible to suppress catalyst deactivation completely by applying low temperatures.

A dimensionless reaction process for the observed second order catalyst deactivation is given by the transformation of eqn (5) into eqn (6).

$$\frac{r_{eff}(t)}{r_{eff,0}} = \frac{1}{1 + r_{eff,0} \cdot k_{d,2} \cdot t} \quad (6)$$

With the known initial reaction rate and rate constant of deactivation the course of the reaction can be predicted. As the deactivation coefficient is not only temperature dependent but also influenced by the partial pressure of ethene, the deactivation coefficient $k_{d,2}$ has to be described as a function of both. In the ESI† we give values for $k_{d,2}$ (in $l$ $mol^{-1}$) as a function of the reaction temperature and the partial pressure of ethene. In Fig. 10 the mathematical modeling of the deactivation process is compared with the measured course of the reaction for the three temperatures 282, 292, and 302 K. The lines reflect the calculated deactivation process for the

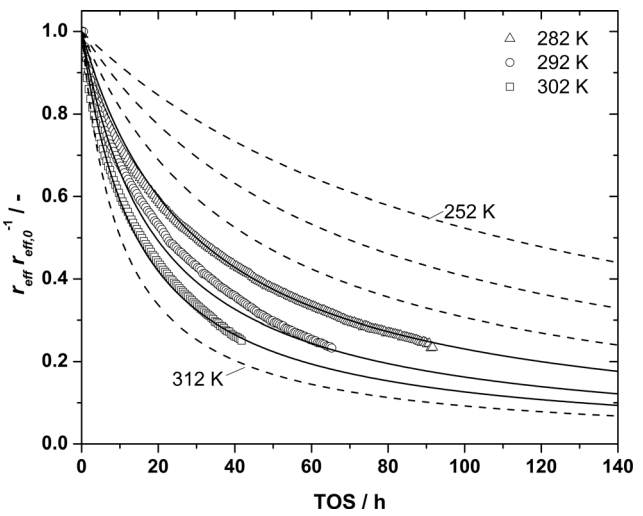


**Fig. 10** Comparison of the mathematical modelling of the catalyst deactivation process with experimental results – the applied model includes a second order deactivation process and an $E_{A,d}$ value of 23.2 kJ $mol^{-1}$. SILP catalysts comprising [(mall)Ni-dppanis][$SbF_6$] **1**, $w_{Ni}$ = 2.50 $mg_{Ni}$ $g_{support}^{-1}$, **S5**, [$C_2C_1$Im][FAP], $\alpha_{IL}$ = 0.3; $m_{SILP}$ = 200 mg, $p_{ethene}$ = 68 mbar, $V_{ethene}$ = 5.1 Nml $min^{-1}$, $t \approx 0.3$ s, and $p_{reaction}$ = 1 bar.

temperatures between 252 and 312 K in steps of 10 K, assuming an almost unchanged initial reaction rate, as we surprisingly found for the temperatures between 282 and 302 K.

The mathematical modeling of the deactivation process fits very well for an assumed second order deactivation process. For comparison, the mismatching fit for an assumed first order deactivation process can be seen in the ESI.† These results illustrate that even for a temperature as low as 252 K the deactivation process of the catalyst would be still significant if the same deactivation mechanism prevails at this low temperature. However, at such low temperatures, condensation of oligomerization products in the SILP catalyst would cause major problems.

## Experimental

All air- and moisture-sensitive experiments and syntheses were carried out in an inert glovebox or under an argon atmosphere using standard Schlenk techniques. 1-Ethyl-3-methylimidazolium tris(pentafluoroethyl)trifluorophosphate $[C_2C_1Im][eFAP]$ (purity ≥99.0%, water content ≤100 ppm, halide content ≤100 ppm) and 1-ethyl-3-methylimidazolium tetrafluoroborate $[C_2C_1Im][BF_4]$ were purchased from Merck KGaA and used without further purification. The Ni catalyst complex $[(mall)Ni\text{-}dppanis][SbF_6]$ (dppanis = (2-methoxyphenyl)diphenylphosphine) that was used in the dimerization of ethene was synthesized by Dr. Nicola Taccardi, Chemical Reaction Engineering, FAU Erlangen-Nuremberg, according to literature known preparation routes. The support materials Carrier 1–4 (**S1**–**S4**) and Spherical A (**S5**) and B (**S6**), were provided by Clariant. The support materials silica 100 (**S7**), silica gel 60 (**S8**) and PharmPrep 60 cc (**S12**) were purchased from Merck. Trisoperl 1200 45–65 μm (**S9**) and 20–35 μm (**S11**) and Trisoperl 500 (80–130 μm) (**S10**) were purchased from VitraBio™. Each of the support materials was calcined prior to application using the following procedure: the support material was heated up from room temperature to 423 K with a heating rate of 4 K $min^{-1}$. In order to remove water out from the pores a temperature of 423 K was kept constant for two hours. Afterwards, the support was heated up to 873 K with a heating rate of 4 K $min^{-1}$. Before the material finally cooled down to room temperature, a temperature of 873 K was maintained for another 12 h. The pretreated material was evacuated overnight and eventually stored in an inert gas box.

The SILP catalysts were prepared by dissolution of the self-activating Ni-methallyl complex and the required amount of ionic liquid in dichloromethane (<0.004% $H_2O$, stabilized with 50.00 ppm 2-methyl-2-butene). After addition of the desired amount of the support material the solvent of the suspension was removed within 30 min at 273 K. The catalyst was cooled for transportation at 273 K and stored in the glovebox at 253 K. The formal pore filling $\alpha_{IL}$ of the SILP catalyst was calculated according to eqn (7).

$$\alpha_{IL} = \frac{V_{IL}}{m_{support} \cdot V_{pore}} \left[ \frac{cm_{IL}^{\ 3} \cdot g_{support}}{g_{support} \cdot cm_{pore}^{\ 3}} \right] \quad (7)$$

The Ni content of the SILP catalysts was calculated according to eqn (8).

$$w_{Ni} = \frac{m_{Ni}}{m_{support}} = \frac{m_{Ni\text{-}precursor} \cdot M_{Ni}}{m_{support} \cdot M_{Ni\text{-}precursor}} \left[ \frac{mg_{Ni}}{g_{support}} \right] \quad (8)$$

In order to investigate the effect of various IL loadings on the stability of the SILP catalyst, samples with pore fillings of $\alpha_{IL}$ = 0.3, 0.6 and 0.9 were prepared. The specific pore volume and the specific BET surface area of the original support materials were determined using a Quantrachrome Quadrasorb SI Micrometrics ASAP instrument. The particle size distribution was measured at the Chair of Particle Technology, FAU Erlangen-Nuremberg using a Malvern Mastersizer 2000. Pressure drop curves were recorded using a GDH precision digital manometer for the pressure range of 0–199.9 mbar. These experiments were conducted in a glass reactor with an inner diameter of 15 mm. The nitrogen flow was adjusted using a mass flow controller in the range of 1–50 ml $min^{-1}$.

All catalytic experiments were conducted within a continuous gas phase reactor built in-house. A schematic view of the dimerization set-up is depicted in Fig. 11.

The gas phase experiments were carried out with ethene (3.5, ≥99.95%, Linde Gas AG) as the substrate for the dimerization and argon (4.8, ≥99.998%, Linde Gas AG) as the inert carrier gas. For additional purification, the ethene feed was cleaned using a high-capacity oxygen trap (Restek) to remove oxygen to less than 15 ppb. We refer to this ethene quality as "purified ethene". Argon was purified using a high-capacity moisture trap (Restek, water content ≤15 ppb) and an aforementioned high-capacity oxygen trap (all experiments except entries 17 and 18). Each gas was dosed *via* a multi range mass flow controller (Bronkhorst). The adjustable volume flow ranged 1–50, 1–100 and 1–150 ml $min^{-1}$. Both gases were mixed in a static mixer and subsequently passed through the double-walled glass reactor either upstream or downstream. Due to flexible connections at the reactor in- and outlets, both operation modes (fixed bed and fluidized bed) could be realized. To reach steady-state conditions the reactor was by-passed. After passing through the reactor the gas stream was analyzed online using a gas chromatograph (Agilent 7820A GC).

In preparation for the dimerization the reactor was evacuated over several hours at 343 K and $1 \times 10^{-2}$ mbar. Afterwards the pressure was adjusted with argon at 292 K. At the beginning of the reaction the cooled SILP-catalyst was filled in the reactor under an argon stream ($V$ = 10 ml $min^{-1}$). In addition the reactor was subsequently purged with argon ($V$ = 100 ml $min^{-1}$) in order to avoid moisture and oxygen contaminants for 2 min and closed afterwards with a slight overpressure of 200 mbar. Before the reaction started the volume flows of ethene and argon were adjusted over the bypass. Reaching continuous flow conditions the bypass was closed and the reactor valves were opened. With the reaction the online measurement was started simultaneously.

 

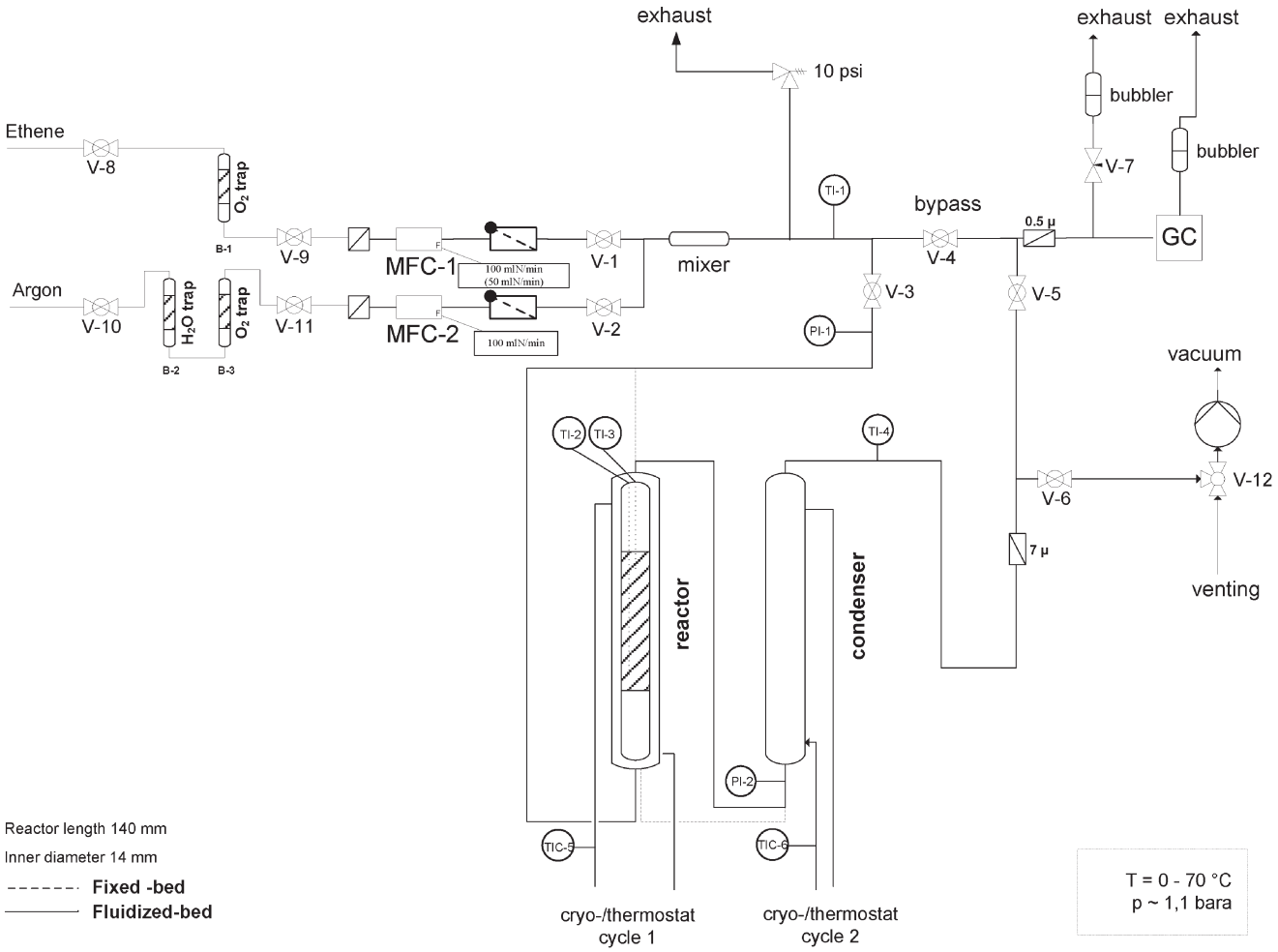


**Fig. 11** Schematic view of the experimental set-up for the gas phase dimerization of ethene in a fluidized bed or fixed bed reactor.

## Conclusion

In this study, we adapted cationic nickel based SILP catalysts in a fluidized bed reaction for the first time. We therefore characterized different $SiO_2$-based porous support materials with regard to their fluidization behavior and monitored the influence of IL loading of the support on the fluidization characteristics. By adding an IL to the support, the minimum fluidization velocity was increased (for pore filling $\alpha_{IL}$ = 0.9 by around 27%) and the overall pressure drop became more pronounced. However, even with a high pore filling of up to 90% fluidization was still possible. We could not observe a major drawback like agglomeration of the SILP catalysts as a result of the IL impregnation. Our catalytic experiments establish that a dilution with an inert gas was required for the dimerization of ethene with cationic Ni SILP-type catalysts in a fluidized bed operation, since a process with pure ethene led to an immediate deactivation by the released reaction heat and an agglomeration of SILP catalysts due to condensation of higher boiling products. The comparison of fixed bed and fluidized bed processes indicated that the improved distribution of the released reaction heat in the latter was advantageous for the stability of the cationic Ni SILP-type catalysts. The investigation of the influence of support materials, pore filling, and reaction temperature on the deactivation behavior of the SILP catalysts showed that higher pore filling degrees gave lower reaction rates and, in consequence, generated less reaction heat. For temperature sensitive nickel catalysts this lower heat generation resulted in prolonged stability. Additionally, an improved removal or distribution of the reaction heat by higher heat conductivity and using thicker ionic liquid films proved advantageous for the reaction.

The variation of the partial pressures of ethene showed opposing trends. With increasing partial pressure the rate of reaction increased, while at the same time deactivation was reduced. We attributed this to a deactivation mechanism of Ni complexes reacting with themselves or impurities when the availability of ethene is low while too high ethene concentrations would result in high reaction rates, thus generating too much heat inside the SILP catalyst pellets.

Applying SILP catalysts in the fluidized bed reactor with its good isothermicity, we were also able to determine the deactivation kinetics of the ethene dimerization with cationic

Ni based SILP catalysts in diluted feed. The activation energy of deactivation for the particular SILP material comprising the Ni-dppanis precursor dissolved in $[C_2C_1Im][FAP]$ ($\alpha_{IL}$ = 0.3 for the support **S5**) was determined to be $E_{A,d}$ = 23.2 kJ mol$^{-1}$. The results indicate that even at temperatures as low as 252 K catalyst deactivation would still be observed if the same catalyst deactivation mechanism prevails. At this temperature, however, product condensation would be a major practical issue. Future work will focus on the development of cationic Ni complexes with higher robustness against temperature and low ethylene pressures. Catalytic oligomerization using SILP catalysts in a fluidized bed reactor has in principle proven to be an interesting and feasible concept.

## Acknowledgements

The authors would like to gratefully thank the Cluster of Excellence "Engineering of Advanced Materials" (EAM) Erlangen-Nuremberg and the Deutsche Forschungsgemeinschaft for funding. Moreover, the authors kindly thank Timo Hensler and Claudia Eisermann from the Chair of Particle Technology, University of Erlangen-Nuremberg for measurements of particle size distribution. The authors also gratefully acknowledge Clariant as a strategic partner within the EAM research initiative for their support and provision of the support materials **S1 to S6**.

## References

1 *Evolving Propylene Sources, Solution to Supply Shortages?*, Chemsystems Prospectus, January 2012.
2 H. Zimmermann and R. Walzl, Ethylene, in *Ullmann's Encyclopedia of Industrial Chemistry*, Wiley-VCH Verlag GmbH & Co. KGaA, 2000.
3 P. Eisele and R. Killpack, Propene, in *Ullmann's Encyclopedia of Industrial Chemistry*, Wiley-VCH Verlag GmbH & Co. KGaA, 2000.
4 (*a*) H. Oikawa, Y. Shibata, K. Inazu, Y. Iwase, K. Murai, S. Hyodo, G. Kobayashi and T. Baba, *Appl. Catal., A*, 2006, **312**, 181–185; (*b*) T. Baba and H. Sawada, *Phys. Chem. Chem. Phys.*, 2002, **4**, 3919–3923.
5 B. Lin, Q. Zhang and Y. Wang, *Ind. Eng. Chem. Res.*, 2009, **48**, 10788–10795.
6 P. P. O'Neill and J. J. Rooney, *J. Am. Chem. Soc.*, 1972, **94**, 4383–4384.
7 J. Engelhardt, *J. Catal.*, 1980, **62**, 243–252.
8 T. Yamaguchi, Y. Tanaka and K. Tanabe, *J. Catal.*, 1980, **65**, 442–447.
9 M. Taoufik, E. Le Roux, J. Thivolle-Cazat and J.-M. Basset, *Angew. Chem., Int. Ed.*, 2007, **46**, 7202–7205.
10 (*a*) M. Iwamoto and Y. Kosugi, *J. Phys. Chem. C*, 2006, **111**, 13–15; (*b*) K. Ikeda, Y. Kawamura, T. Yamamoto and M. Iwamoto, *Catal. Commun.*, 2008, **9**, 106–110; (*c*) M. Iwamoto, *Molecules*, 2011, **16**, 7522–7550.
11 T. Lehmann, T. Wolff, V. M. Zahn, P. Veit, C. Hamel and A. Seidel-Morgenstern, *Catal. Commun.*, 2011, **12**, 368–374.
12 J. Scholz, V. Hager, X. Wang, F. T. U. Kohler, M. Sternberg, M. Haumann, N. Szesni, K. Meyer and P. Wasserscheid, *ChemCatChem*, 2014, **6**, 162–169.
13 I. Brassat, W. Keim, S. Killat, M. Möthrath, P. Mastrorilli, C. F. Nobile and G. P. Suranna, *J. Mol. Catal. A: Chem.*, 2000, **157**, 41–58.
14 F. Speiser, P. Braunstein and L. Saussine, *Acc. Chem. Res.*, 2005, **38**, 784–793.
15 U. Müller, W. Keim, C. Krüger and P. Betz, *Angew. Chem., Int. Ed. Engl.*, 1989, **28**, 1011–1013.
16 G. Wilke, *Angew. Chem., Int. Ed. Engl.*, 1988, **27**, 185–206.
17 P. J. Flory, *J. Am. Chem. Soc.*, 1940, **62**, 1561–1565.
18 R. B. A. Pardy and I. Tkatchenko, *J. Chem. Soc., Chem. Commun.*, 1981, 49–50.
19 (*a*) D. Matt, M. Huhn, J. Fischer, A. De Cian, W. Kläui, I. Tkatchenko and M. C. Bonnet, *J. Chem. Soc., Dalton Trans.*, 1993, 1173; (*b*) P. Kuhn, D. Sémeril, C. Jeunesse, D. Matt, P. Lutz and R. Welter, *Eur. J. Inorg. Chem.*, 2005, 1477–1481; (*c*) P. Kuhn, D. Sémeril, C. Jeunesse, D. Matt, M. Neuburger and A. Mota, *Chem.–Eur. J.*, 2006, **12**, 5210–5219.
20 (*a*) K. Hirose and W. Keim, *J. Mol. Catal.*, 1992, **73**, 271–276; (*b*) W. Keim and R. P. Schulz, *J. Mol. Catal.*, 1994, **92**, 21–33; (*c*) J. Heinicke, M. He, A. Dal, H.-F. Klein, O. Hetche, W. Keim, U. Flörke and H.-J. Haupt, *Eur. J. Inorg. Chem.*, 2000, 431–440; (*d*) J. Heinicke, M. Köhler, N. Peulecke and W. Keim, *J. Catal.*, 2004, **225**, 16–23.
21 (*a*) J. Pietsch, P. Braunstein and Y. Chauvin, *New J. Chem.*, 1998, **22**, 467–472; (*b*) P. Braunstein, Y. Chauvin, S. Mercier and L. Saussine, *C. R. Chim.*, 2005, **8**, 31–3.
22 Z. J. A. Komon, X. Bu and G. C. Bazan, *J. Am. Chem. Soc.*, 2000, **122**, 1830–1831.
23 J. M. Malinoski and M. Brookhart, *Organometallics*, 2003, **22**, 5324–5335.
24 I. Brassat, W. Keim, S. Killat, M. Möthrath, P. Mastrorilli, C. F. Nobile and G. P. Suranna, *J. Mol. Catal. A: Chem.*, 2000, **157**, 41–58.
25 M. C. Bonnet, F. Dahan, A. Ecke, W. Keim, R. P. Schulz and I. Tkatchenko, *J. Chem. Soc., Chem. Commun.*, **1994**, 615–616.
26 R. F. de Souza, K. Bernardo-Gusmão, G. A. Cunha, C. Loup, F. Leca and R. Réau, *J. Catal.*, 2004, **226**, 235–239.
27 (*a*) Y. Chauvin, B. Gilbert and I. Guibard, *J. Chem. Soc., Chem. Commun.*, 1990, 1715–1716; (*b*) Y. Chauvin, S. Einloft and H. Olivier, *Ind. Eng. Chem. Res.*, 1995, **34**, 1149–1155; (*c*) Y. Chauvin, H. Olivier, C. N. Wyrvalski, L. C. Simon and R. F. de Souza, *J. Catal.*, 1997, **165**, 275–278.
28 H. Olivier and P. Laurent-Gérot, *J. Mol. Catal. A: Chem.*, 1999, **148**, 43–48.
29 (*a*) L. C. Simon, J. Dupont and R. F. de Souza, *Appl. Catal., A*, 1998, **175**, 215–220; (*b*) K. Bernardo-Gusmão, L. F. Trevisian Queiroz, R. F. de Souza, F. Leca, C. Loup and R. Réau, *J. Catal.*, 2003, **219**, 59–62.
30 B. Ellis, W. Keim and P. Wasserscheid, *Chem. Commun.*, 1999, 337–338.
31 (*a*) C. P. Mehnert, R. A. Cook, N. C. Dispenziere and M. Afeworki, *J. Am. Chem. Soc.*, 2002, **124**, 12932–12933; (*b*)

 

C. P. Mehnert, E. J. Mozeleski and R. A. Cook, *Chem. Commun.*, 2002, 3010–3011.

32 A. Riisager, R. Fehrmann, S. Flicker, R. van Hal, M. Haumann and P. Wasserscheid, *Angew. Chem., Int. Ed.*, 2005, **44**, 815–819.

33 For recent reviews see: (*a*) Y. Gu and G. Li, *Adv. Synth. Catal.*, 2009, **351**, 817–847; (*b*) C. Van Doorslaer, J. Wahlen, P. Mertens, K. Binnemans and D. De Vos, *Dalton Trans.*, 2010, **39**, 8377–8390; (*c*) J. Scholz and M. Haumann, Supported Ionic Liquid Thin Film Technology, in *Nanomaterials in Catalysis*, ed. P. Serp and K. Philippot, Wiley-VCH Verlag GmbH & Co. KGaA, 2013.

34 (*a*) F. Kohler, D. Roth, E. Kuhlmann, P. Wasserscheid and M. Haumann, *Green Chem.*, 2010, **12**, 979–984; (*b*) S. Werner, N. Szesni, M. Kaiser, R. W. Fischer, M. Haumann and P. Wasserscheid, *ChemCatChem*, 2010, **2**, 1399–1402; (*c*) M. Jakuttis, A. Schönweiz, S. Werner, R. Franke, K.-D. Wiese, M. Haumann and P. Wasserscheid, *Angew. Chem., Int. Ed.*, 2011, **50**, 4492–4495.

35 A. Berkefeld and S. Mecking, *J. Am. Chem. Soc.*, 2009, **131**, 1565–1574.

36 K. Noda, S. Uchida, T. Makino and H. Kamo, *Powder Technol.*, 1986, **46**(2–3), 149–54.

37 S. K. Gupta, V. K. Agarwal, S. N. Singh, V. Seshadri, David Mills, J. Singh and Chandra Prakash, *Powder Technol.*, 2009, **196**(3), 263–271.

38 D. Geldart, *Powder Technol.*, 1973, **7**(5), 285–292.